AGU ADVANCING EARTH AND SPACE SCIENCE

Geophysical Research Letters

RESEARCH LETTER
10.1029/2020GL090328

Special Section:
The Exceptional Arctic Polar Vortex in 2019/2020: Causes and Consequences

Seasonal Forecasts of the Exceptional Northern Hemisphere Winter of 2020

Simon H. Lee[1], Zachary D. Lawrence[2,3], Amy H. Butler[4], and Alexey Y. Karpechko[5]

[1]Department of Meteorology, University of Reading, Reading, UK, [2]Cooperative Institute for Research in Environmental Sciences (CIRES), University of Colorado, Boulder, CO, USA, [3]NOAA Physical Sciences Laboratory (PSL), Boulder, CO, USA, [4]NOAA Chemical Sciences Laboratory (CSL), Boulder, CO, USA, [5]Finnish Meteorological Institute, Helsinki, Finland

Abstract The winter of 2019–2020 was dominated by an extremely strong stratospheric polar vortex and positive tropospheric Arctic Oscillation (AO). Here, we analyze forecasts from six different prediction systems contributing to the C3S seasonal forecast database. Most performed very strongly, with consistently high skill for January–March 2020 from forecasts launched through October–December 2019. Although the magnitude of the anomalies was underestimated, the performance of most prediction systems was extremely high for a positive AO winter relative to the common hindcast climate. Ensemble members which better predicted the extremely strong stratospheric vortex better predicted the extreme tropospheric state. We find a significant relationship between forecasts of the anomalous midlatitude tropospheric wave pattern in early winter, which destructively interfered with the climatological stationary waves and the strength of the stratospheric vortex later in the winter. Our results demonstrate a strong interdependence between the accuracy of stratospheric vortex and AO forecasts.

Plain Language Summary Westerly winds during the winter of 2019–2020 were unusually strong and long lasting through a deep layer of the atmosphere. We investigate how well this was predicted months ahead of time. We find that seasonal weather forecast systems predicted the winter pattern very well, especially when compared with previous winters. Forecasts which better predicted the strength of the winds higher in the atmosphere did better overall. We find that there was a link between predictions of the weather patterns lower down in the atmosphere and how they suppressed large-scale atmospheric waves in the midlatitudes, which likely helped the winds remain stronger higher up.

Key Points:
- Forecasts from six seasonal prediction systems consistently predicted the large-scale winter patterns with unusually high accuracy
- Ensemble members which better predicted the extreme stratospheric state also better predicted the extreme tropospheric state
- Accurate prediction of the midlatitude tropospheric wave pattern was associated with more accurate stratospheric forecasts

Supporting Information:
- Supporting Information S1

Correspondence to:
S. H. Lee,
s.h.lee@pgr.reading.ac.uk

Citation:
Lee, S. H., Lawrence, Z. D., Butler, A. H., & Karpechko, A. Y. (2020). Seasonal forecasts of the exceptional Northern Hemisphere winter of 2020. *Geophysical Research Letters*, *47*, e2020GL090328. https://doi.org/10.1029/2020GL090328

Received 12 AUG 2020
Accepted 4 OCT 2020
Accepted article online 17 OCT 2020

1. Introduction

The Northern Hemisphere (NH) winter of 2019–2020, particularly January–March (JFM) 2020, was characterized by a strong and persistent positive phase of the Arctic Oscillation (AO) (Hardiman et al., 2020; Lawrence et al., 2020)—the leading mode of extratropical tropospheric wintertime variability, analogous to the surface Northern Annular Mode (NAM) (e.g., Black & McDaniel, 2004; Thompson & Wallace, 1998, 2001) and closely related to the North Atlantic Oscillation (NAO) (Feldstein & Franzke, 2006). The magnitude and persistence of this pattern, associated with strengthened and poleward-shifted extratropical storm tracks, led to unusually warm conditions across NH midlatitudes, as well as hydrometeorological extremes associated with the shifted storm tracks. For example, while the United Kingdom experienced its wettest February since at least 1862, Spain experienced its driest February in at least 56 years (NOAA, 2020). Coupled to the strongly positive tropospheric NAM was an extremely strong stratospheric polar vortex (SPV) (Lawrence et al., 2020); significant disturbances to the SPV, so-called sudden stratospheric warmings (SSWs) (e.g., Butler et al., 2015; Charlton & Polvani, 2007), were entirely absent during their climatological peak of January–March. The record-cold temperatures within the undisturbed SPV led to unprecedented ozone loss over the Arctic during spring 2020 (Manney et al., 2020; Wohltmann et al., 2020). Thus, the winter of 2020 represents a vertically deep, extreme climatic state, which offers a rare opportunity to test the performance of operational seasonal forecast models in predicting such an extreme.

Seasonal forecast models have demonstrated significant skill in predicting large-scale wintertime climate modes such as the NAO/AO (Scaife et al., 2014), though with significant year-to-year variability.

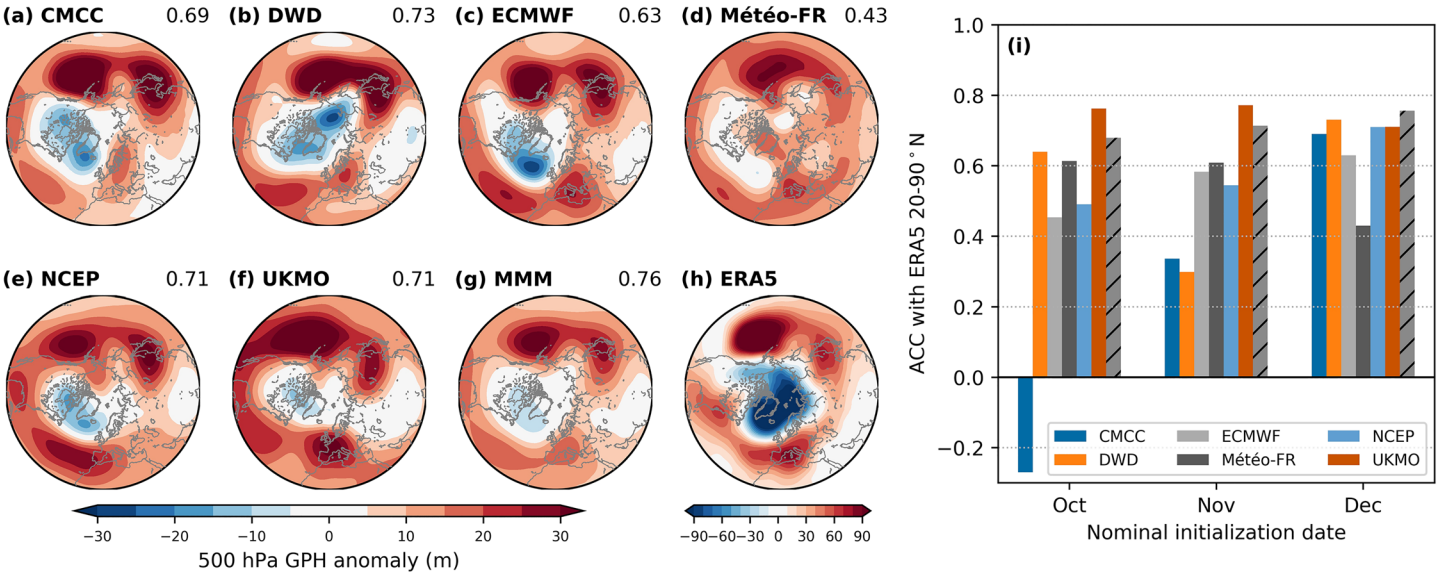

Figure 1. (a–f) Average January–March 2020 ensemble-mean 500 hPa geopotential height (Z500 GPH) anomalies, poleward of 20°N, from six seasonal prediction systems nominally initialized on 1 December 2019. Anomalies are expressed with respect to the 1993–2016 hindcast climatology for each prediction system. (g) Multimodel mean (MMM) of a–f. (h) As in panels a–g but for ERA5 reanalysis. Due to the larger anomaly magnitudes in ERA5, a separate color scale is used. The number in the top right of panels a–g indicates the anomaly correlation coefficient (ACC) with ERA5. (i) ACC between ensemble-mean JFM-mean Z500 anomalies poleward of 20°N and ERA5, for nominal initialization dates of October, November, and December 2019. The MMM is shown as a hatched bar.

A component of this predictability may arise from the SPV state at the start of the winter (Nie et al., 2019) and accurate predictions of the likelihood of extreme SPV states during the winter (both strong vortex events and SSWs) due to their relatively long persistence (Scaife et al., 2016). Additional influences on the seasonal-mean NAO/AO and SPV include tropical sea surface temperatures (SSTs) and precipitation, including the El Niño-Southern Oscillation (ENSO) and Indian Ocean SSTs (Baker et al., 2019; Domeisen et al., 2019; Fletcher & Cassou, 2015; Hall et al., 2017; Trascasa-Castro et al., 2019), Atlantic SSTs (Hall et al., 2017; Rodwell & Folland, 2002; Wang et al., 2004) and North Pacific SSTs (Hurwitz et al., 2012). These can interact directly through forcing tropospheric Rossby wave trains, or indirectly by influencing the strength of the SPV (e.g., Ineson & Scaife, 2009) through modulation of vertically propagating wave activity. Some of the aforementioned drivers have been used with some success in statistical forecasts (e.g., Folland et al., 2012; Hall et al., 2017; Riddle et al., 2013; Wang et al., 2017) to elucidate sources of predictability in dynamical models.

In this letter, we analyze how well the extreme large-scale circulation patterns present during winter (JFM) 2020 were predicted by seasonal forecasts issued during late 2019 from different prediction systems. We assess whether forecasts that more accurately captured the SPV strength better captured the strength of the positive tropospheric AO and overall NH pattern, given their close statistical and dynamical link. We also investigate possible drivers of the extreme winter pattern.

2. Data and Methods

We analyze data from six prediction systems that contribute to the Copernicus Climate Change Service (C3S) seasonal forecast database—namely, from the United Kingdom Met Office (UKMO), the European Centre for Medium-range Weather Forecasts (ECMWF), Météo-France, Deutsche Wetterdeinst (DWD), the National Centers for Environmental Prediction (NCEP), and the Euro-Mediterranean Center on Climate Change (Centro euro-Mediterraneo sui Cambiamenti Climatici, CMCC). Data are provided at 1° latitude-longitude resolution. As stratospheric-level data from NCEP are not currently available from C3S, it is not included in the multimodel comparison for that part of the analysis. Table S1 in the supporting information provides details of the individual model systems used. All model anomalies are expressed with respect to the common hindcast initialization period 1993–2016. Additionally, the multimodel mean

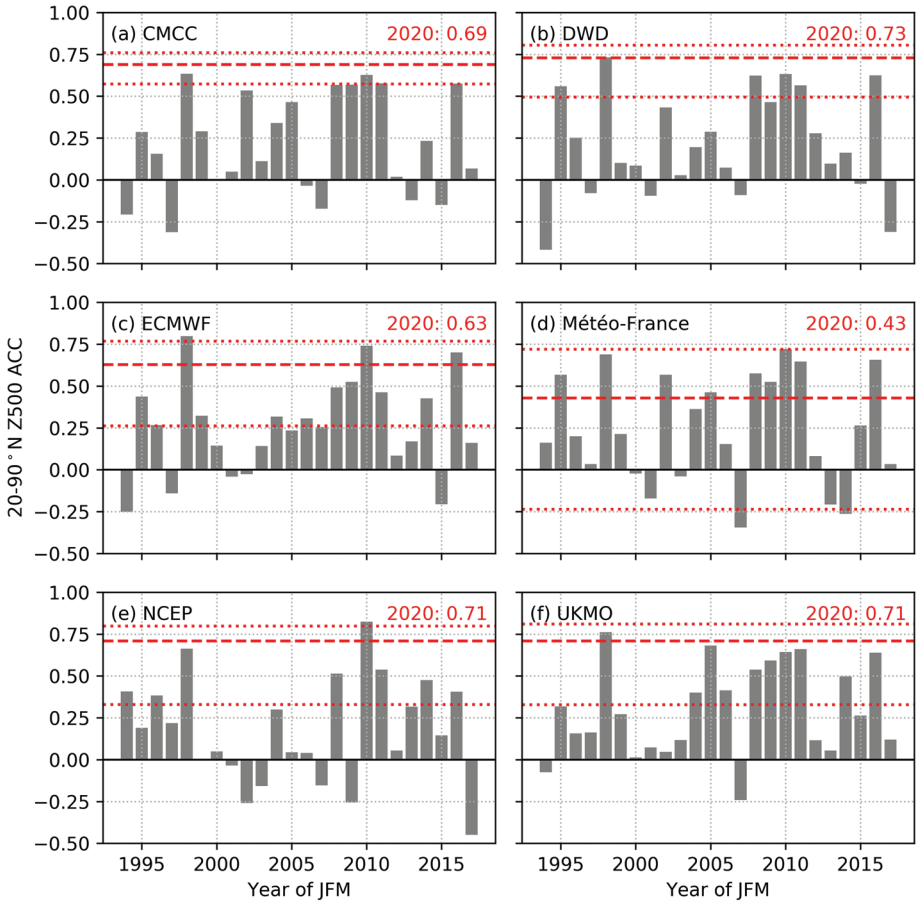

Figure 2. ACCs (gray bars) between ensemble-mean JFM-mean Z500 poleward of 20°N and ERA5 for nominal 1 December hindcasts in the common period 1993–2016. Dashed red lines are the respective ACCs from the December 2019 forecast; dotted red lines indicate the 95% confidence interval obtained by resampling the forecast ensemble to the size of the hindcast ensemble 10,000 times (without replacement).

(MMM) is calculated as the average of the ensemble means of the six models. Verification is performed with the ECMWF ERA5 reanalysis at 1.0° resolution (Hersbach et al., 2020), with anomalies computed with respect to the monthly December 1993 to March 2017 climatology.

The anomaly correlation coefficient (ACC) (e.g., Wilks, 2019) over a domain between a forecast anomaly $f$at each grid point i and j and corresponding observation o, weighted by cosine-latitude w, is calculated using

$$ACC = \frac{cov(f,\, o;\, w)}{\sqrt{cov(f, f;\, w)\, cov(o,\, o;\, w)}}, \tag{1}$$

where the weighted covariance is calculated as

$$cov(f,\, o;\, w) = \frac{\sum_i \sum_j w_{i,j} (f_{i,j} - \overline{f_w})\,(o_{i,j} - \overline{o_w})}{\sum_i \sum_j w_{i,j}}, \tag{2}$$

where the overbar indicates the weighted average across the domain.

The AO index is computed as the leading empirical orthogonal function (EOF) of JFM-averaged mean sea level pressure (MSLP) anomalies poleward of 20°N (e.g., Thompson & Wallace, 1998) over the period December 1993–March 2017 in ERA5, which explains 27% of the total variance. Anomalies are weighted

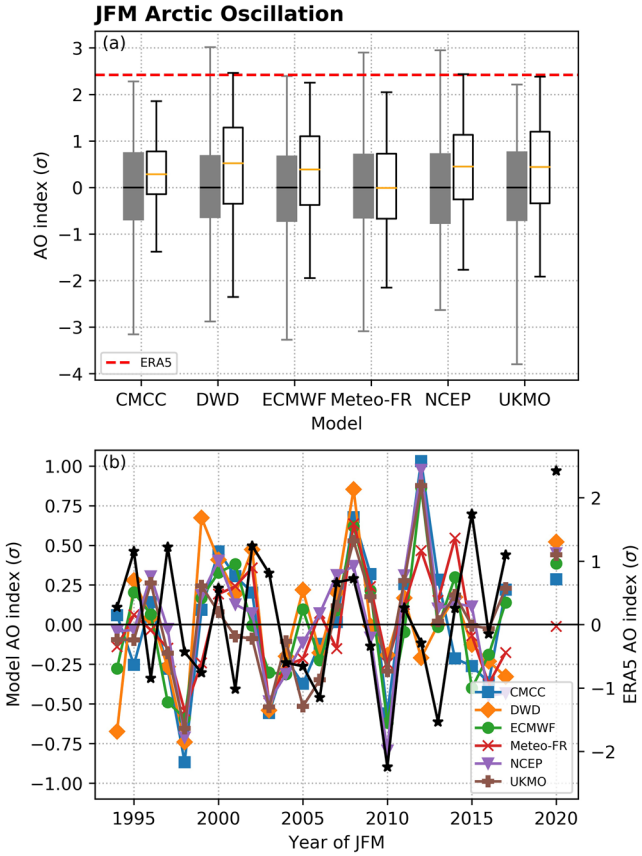

Figure 3. (a) Forecasts of the average JFM 2020 Arctic Oscillation (non-filled boxes), for 6 seasonal prediction systems nominally initialized on 1 December 2019. Solid gray boxes show the corresponding hindcast distribution for JFM 1994-2017. Horizontal lines indicate the mean. Whiskers extend to the extreme values. The observed anomaly from ERA5 (2.4 σ) is shown with a horizontal red line. Units are standard deviations of the corresponding hindcast/reanalysis climatology. (b) Ensemble-mean AO hindcasts for JFM 1994–2017 (left-hand ordinate) and ERA5 (right-hand ordinate). The ensemble-mean forecasts and ERA5 for JFM 2020 are also shown.

by the square-root of cosine-latitude to give equal area weighting. In the seasonal forecasts and the ERA5 verification, the forecast AO index is computed as the projection of the ERA5 EOF onto the forecast/reanalysis MSLP anomalies and is scaled to have unit standard deviation (across all ensemble members) over the hindcast period in each model and ERA5.

3. Tropospheric Forecasts

We first assess the skill of the seasonal forecasts by considering predictions of the extratropical midtropospheric flow. Aside from regional subtleties, Figure 1 shows that all systems predicted strikingly similar patterns on the hemispheric scale—both with each other and with ERA5, though with characteristically low signal amplitude (e.g., Scaife et al., 2014). The similarity with ERA5 is reflected in the high ACCs, which exceed 0.6 for all but Météo-France (0.43) and otherwise range from 0.63 (ECMWF) to 0.73 (DWD) for the individual prediction systems, while the MMM performed the best (0.76). There are several key features of the observed wintertime state (Figure 1h): (i) a strongly positive NAO pattern, with an enhanced poleward height gradient in the Atlantic sector, (ii) a large anomalous ridge in the northeast Pacific, and (iii) a secondary ridge anomaly in eastern Asia and the northwest Pacific. All systems predicted the Pacific ridge anomalies, though in Météo-France only one broad anomalous ridge was predicted. All but Météo-France predicted the enhanced Iceland low and Azores high characteristic of the positive NAO.

Another feature of the seasonal forecasts of winter 2020 was their general consistency in predicting a similar pattern across different initializations. Equivalent maps as Figure 1 but for October and November forecasts are provided in the supporting information (Figures S1 and S2). For brevity, we show the ACCs for these forecasts in Figure 1i. The highest-performing forecasts were the October and November forecasts from UKMO, which had ACCs of 0.76 and 0.77, respectively. The MMM performed very strongly across the initialization dates despite considerable intermodel differences, with an ACC of 0.68–0.76, only exceeded by the forecasts from UKMO in October and November. The lowest-performing forecasts were the October initialization from CMCC (−0.27) and both October and November initializations from CMCC (0.34) and DWD (0.30). In these cases, a notable missing feature was the anomalous ridge in the northeast Pacific.

The ACC skill of the forecasts for winter 2020 was unusually high with respect to the common hindcast period. Figure 2 shows the JFM ACCs for hindcasts nominally initialized on 1 December 1993–2016, alongside the ACC for the 2020 forecast. As the operational forecast ensemble sizes are larger than the hindcast ensembles (c.f. Table S1), we also show a 95% confidence interval around the 2020 forecast obtained by randomly sub-sampling the operational forecast ensemble to the size of the hindcast ensemble 10,000 times. When accounting for this uncertainty, the performance of all systems except Météo-France exceeded more than half of the hindcast years; without the uncertainty estimate the skill of the full ensemble exceeded most years. Only JFM 1998 and 2010 lie within the confidence interval for CMCC, the lowest resolution model; unlike 2020, both were significant El Niño years, and neither were positive AO/NAO winters (2010 in fact was dominated by an extremely *negative* AO/NAO). We also note that the mean of the resampled ACCs was systematically smaller than the ACCs of the full ensemble (not shown), consistent with the need for large ensemble sizes to produce skillful forecasts (Scaife et al., 2014).

As suggested by Figure 1, all but Météo-France predicted a positive AO for JFM 2020 (Figure 3a). However, the ensemble-mean forecasts were around 0.5 σ, much less than the observed value of 2.4 σ; only the

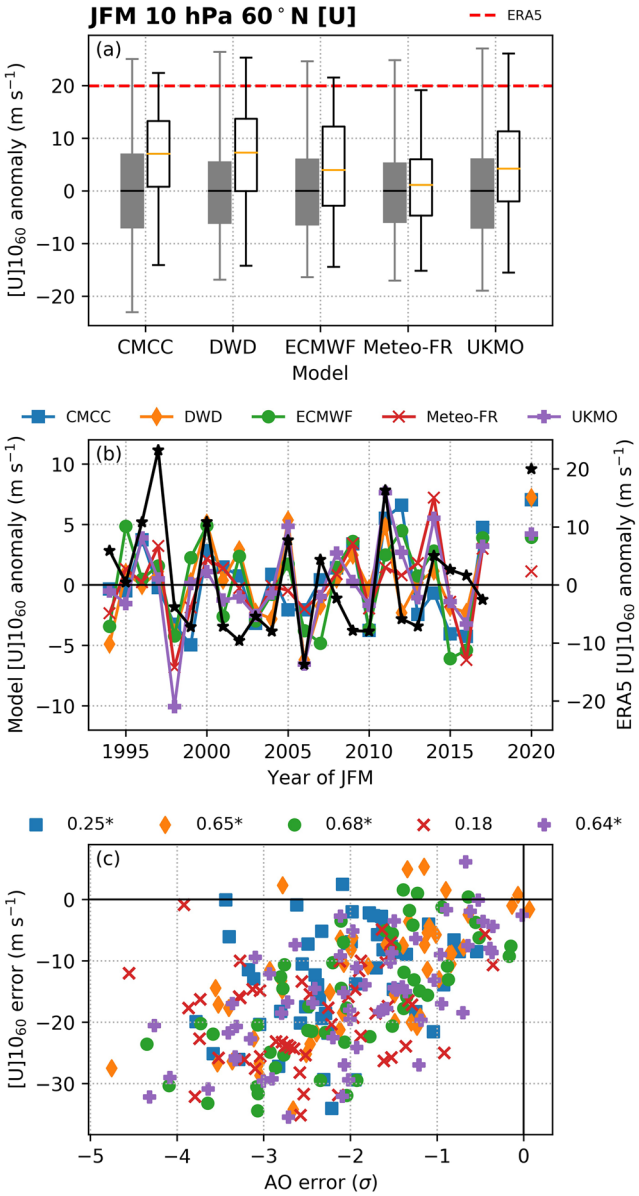

Figure 4. (a, b) As in Figure 3 but for the zonal-mean zonal wind anomaly at 10 hPa and 60°N, excluding forecasts from NCEP. (c) Scatter plot of individual ensemble member forecasts of the JFM 2020 AO and [U]10_{60}, as departures from the ERA5 value. Correlation values are shown, and an asterisk indicates the correlation is significant at the 95% confidence level after 10,000 bootstrap resamples with replacement.

ensemble spread of DWD and NCEP contained the true value. The lack of an ensemble-mean signal for a positive AO in Météo-France is consistent with its lower hemispheric ACC (cf. Figure 1d). The highest observed JFM-mean AO index during 1994–2017 is 1.7 σ in JFM 2015; thus, there is not a similar year within the common hindcast period with which we can compare 2020. The upper-tail of the UKMO predictions lay outside the model hindcast climatology and was thus the only prediction system with ensemble members predicting a record-positive AO. Additionally, Figure 3b shows that, in contrast with ERA5, the ensemble-mean AO index was not a record for any of the models with respect to their hindcasts.

4. SPV Forecasts

We next consider predictions of the seasonal-mean SPV, defined as the JFM-averaged zonal-mean zonal wind at 10 hPa and 60°N (following, e.g., Charlton & Polvani, 2007). Boxplots of the ensemble distributions from the December 2019 initializations, along with the corresponding hindcast distribution, are shown in Figure 4a. The verifying anomaly according to ERA5 was 20.0 m s^{-1}; this is only exceeded by JFM 1997 (23.2 m s^{-1}) in the hindcast period. The ensemble-mean of all systems shown here predicted a stronger-than-average SPV with respect to their own climatological mean state (although the departure was very small for Météo-France), with the greatest departure predicted by DWD (7.2 m s^{-1}). Similarly, the true anomaly magnitude lay within the ensemble spread of all except Météo-France. Figure 4b shows that the ensemble-mean forecasts for JFM 2020 from both CMCC and DWD exceeded any equivalent in their hindcast periods indicating there was an exceptional ensemble-mean signal from these prediction systems for a strong seasonal-mean SPV. This is in contrast to the ensemble-mean AO forecasts, which were not a record with respect to the hindcast period for any prediction system.

We further assess the relationship between the accuracy of SPV forecasts with the accuracy of the AO to assess whether accurate predictions of the anomalous SPV strength were associated with more accurate predictions of the large-scale tropospheric state. Figure 4c shows that, in all but Météo-France, there was a significant positive correlation between the AO error and the SPV error; ensemble members with a stronger SPV tended to have a more positive AO. This linear relationship was strongest in ECMWF ($r = 0.68$), DWD ($r = 0.65$), and UKMO ($r = 0.64$). The lack of a significant correlation in Météo-France is interesting given it predicted both the weakest SPV and least-positive AO. Thus, the linear relationship between the AO and SPV was only evident in the prediction systems which indicated an increased likelihood of a stronger SPV (cf. Figure 5a).

As seasonal-mean statistics may mask subseasonal variability, we also compute the probability of strong or weak SPV events using daily data from the December forecasts and compare with the climatological likelihood. The threshold for a strong/weak vortex is set at the 80th/20th percentiles of the daily hindcast zonal wind distribution for JFM 1994–2017 in each model. We apply a relatively long persistence criterion of 5 days to capture anomalous SPV states with potentially higher seasonal impact. Figure 5a shows that, for all but Météo-France, the probability of a strong vortex in JFM 2020 was significantly elevated with respect to the mean over the JFM 1994–2017 hindcast climate. Correspondingly, the probability of a weak vortex was reduced (Figure 5b). Forecasts from DWD indicated a significantly greater probability of a strong vortex than any winter in the hindcasts. CMCC nominally indicated a lower chance of a weak vortex than any winter in

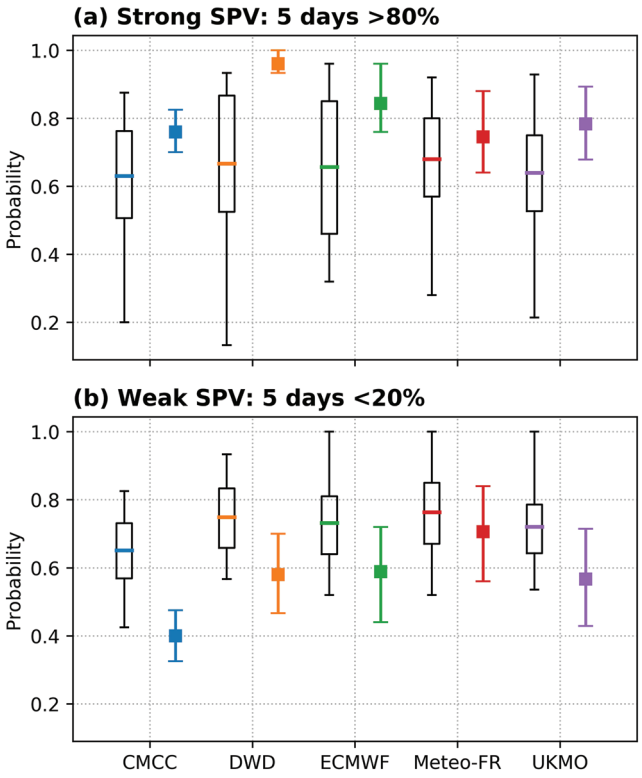

Figure 5. Probability of (a) strong and (b) weak vortex events for JFM from nominal 1 December initializations, using thresholds based on the hindcast climate in each model. Boxplots indicate the hindcast distribution, with the mean indicated by the horizontal line. Squares indicate the probability for JFM 2020. Error bars are a 95% uncertainty estimate by resampling the operational ensemble to the size of the hindcast ensemble 10,000 times (without replacement).

the hindcast period, but the effect of the different ensemble sizes means this difference was not significant. These results are consistent with Figure 4b. Moreover, the absence of a significant departure in the likelihood of a strong or weak vortex in Météo-France is in agreement with its poorer ACC and the absence of a signal for a strongly positive AO.

5. Linking Tropospheric and Stratospheric Forecasts

In this final section we seek to link features in the tropospheric forecasts with those in the stratosphere, using lagged linear regression between different variables across all members of a multimodel ensemble (also known as "ensemble sensitivity analysis," e.g., Dacre & Gray, 2013). First, the individual ensemble mean is subtracted from each ensemble member to produce a perturbation anomaly, and then scaled by the ensemble standard deviation, before then forming the multimodel ensemble. The resultant linear regression coefficients are thus in units of standard deviation of the "response" (leading) variable per standard deviation in the "precursor" variable.

The relationship between 500 hPa geopotential height (Z500) anomalies in January and the February–March SPV strength is shown in Figure 6a. The hemispheric-wide pattern of the regression coefficients is similar to both the ERA5 verification and the forecasts with the highest ACCs in Figure 1, exhibiting significant destructive interference with the climatological-mean eddy height field. The destructive interference that was related to forecasts of a stronger SPV was particularly strong in the North Pacific (destructively interfering with the climatological Aleutian low), western North America, and northeastern Scandinavia and the Ural mountains region. The absence of blocking in the Ural region is in contrast to the SSW precursor patterns (e.g., Karpechko et al., 2018; Lee et al., 2019; Peings, 2019). Similar, albeit weaker, results are found when using Z500 in December and JFM SPV forecasts (not shown). These results are consistent with Lawrence et al. (2020), who found that low vertically propagating tropospheric wave activity was present during the winter.

We also show in Figure 6b that ensemble members which predicted a stronger SPV in January tended to predict a tropospheric anomaly pattern consistent with the positive AO/NAO during February–March, in agreement with Figure 4c. The strongest sensitivity of the FM Z500 anomalies to January SPV strength is over the North Atlantic, where the downward influence of the stratosphere on the troposphere has been found to dominate (Hitchcock & Simpson, 2014). The results in Figure 6 cannot be used to infer causality behind the anomalies in Figure 1 but do suggest that the spread in seasonal forecasts depended on how well the prediction systems captured the two-way coupling process. In particular, these results suggest that both the accurate prediction of certain midlatitude tropospheric anomalies in early midwinter was important in the subsequent prediction of the extremely strong SPV (through suppression of the mean wave field) and that a stronger SPV in early midwinter was associated with a more positive AO later in the winter, likely through downward coupling of persistent stratospheric anomalies.

6. Summary

In this letter, we have analyzed the performance of forecasts for the exceptional winter of 2020 from 6 seasonal prediction systems which contribute to the C3S seasonal forecast database. Our results show that the performance of the majority of the models in predicting the extratropical anomaly pattern was among the highest in the common hindcast period, particularly for a positive AO winter in the absence of a major

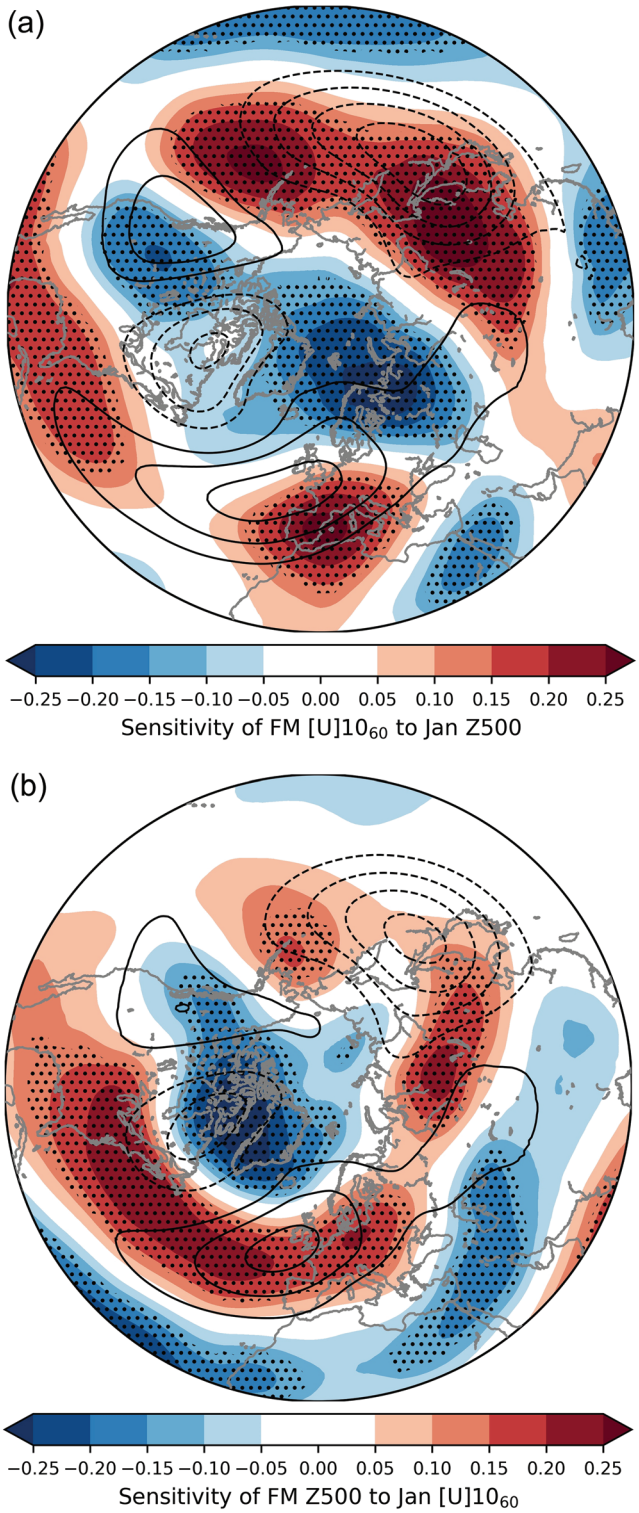

Figure 6. Ensemble sensitivity, across all ensemble members (except NCEP) from the 1 December 2019 initialization, between forecasts of (a) January Z500 and February–March (FM) [U]10$_{60}$ and (b) January [U]10$_{60}$ and FM Z500. Units are standardized departures from the ensemble mean. The corresponding 1994–2017 average eddy height field from ERA5 is shown in contours (every 50 m from -200 to 200 m, excluding 0). Stippling indicates significance at the 95% confidence level after 10,000 bootstrap resamples (with replacement).

ENSO event. We also find that, despite large differences between individual models, the multimodel mean had the most consistently high skill—supporting the usefulness of a multimodel approach. Otherwise, the most consistently skillful forecasts were from UKMO. Of the forecasts from December 2019, only Météo-France did not predict the positive AO or strong SPV and accordingly had the lowest extratropical skill (though earlier initializations performed better, cf. Figures S1 and S2). Although the forecasts systematically underestimated the extreme magnitude of the anomalous AO, the ensemble-mean SPV forecasts from CMCC and DWD exceeded any winter in their hindcasts, indicating the relatively extreme state was predicted by these models.

We further find that ensemble members that predicted a stronger SPV also predicted a stronger AO, suggesting that the prediction of the strong SPV also played a role in accurate predictions of the large-scale surface circulation pattern, consistent with Scaife et al. (2016). For all systems except Météo-France, there were significant increases in the probability of a strong SPV and a decreased probability of a weak SPV/SSW —though these were generally not exceptional with respect to the hindcast period. Nevertheless, this shows that these seasonal forecasts correctly indicated the shift in the likelihood of these subseasonal phenomena.

An ensemble sensitivity analysis showed that ensemble members that predicted greater destructive interference with the tropospheric stationary waves in early winter predicted a stronger SPV later in the winter, in a pattern concordant with the overall anomaly field during winter 2020. This result suggests a two-way relationship between the troposphere and stratosphere during the winter. Modeling experiments, following those of Hardiman et al. (2020) who tied NAO predictability to the Indian Ocean Dipole event in late 2019, will likely be required to fully elucidate the cause of this tropospheric predictability and ascertain why it was better captured by some prediction systems at much longer lead times than others.

Data Availability Statement

The C3S seasonal forecast database and ERA5 reanalysis are available online through the Copernicus Climate Data Store (at https://cds.climate.copernicus.eu/). Operational C3S forecast products are available online (at https://climate.copernicus.eu/charts/c3s_seasonal/).

Acknowledgments

S. H. L. acknowledges funding by the Natural Environment Research Council (NERC) via the SCENARIO Doctoral Training Partnership (NE/L002566/1). Z. D. L. acknowledges support from Federally Appropriated Funds. A. Y. K. acknowledges funding from the Academy of Finland (Project Number 286298). We thank two anonymous reviewers for their helpful comments which improved the paper.

References

Baker, H. S., Woollings, T., Forest, C. E., & Allen, M. R. (2019). The linear sensitivity of the north atlantic oscillation and eddy-driven jet to SSTs. *Journal of Climate*, *32*(19), 6491–6511. https://doi.org/10.1175/JCLI-D-19-0038.1

Black, R. X., & McDaniel, B. A. (2004). Diagnostic case studies of the northern annular mode. *Journal of Climate*, *17*(20), 3990–4004. https://doi.org/10.1175/1520-0442(2004)017<3990:DCSOTN>2.0.CO;2

Butler, A. H., Seidel, D. J., Hardiman, S. C., Butchart, N., Birner, T., & Match, A. (2015). Defining sudden stratospheric warmings. *Bulletin of the American Meteorological Society*, *96*(11), 1913–1928. https://doi.org/10.1175/BAMS-D-13-00173.1

Charlton, A. J., & Polvani, L. M. (2007). A new look at stratospheric sudden warmings. Part I: Climatology and modeling benchmarks. *Journal of Climate*, *20*(3), 449–469. https://doi.org/10.1175/JCLI3996.1

Dacre, H. F., & Gray, S. L. (2013). Quantifying the climatological relationship between extratropical cyclone intensity and atmospheric precursors. *Geophysical Research Letters*, *40*, 2322–2327. https://doi.org/10.1002/grl.50105

Domeisen, D. I. V., Garfinkel, C. I., & Butler, A. H. (2019). The teleconnection of El Niño Southern Oscillation to the stratosphere. *Reviews of Geophysics*, *57*(1), 5–47. https://doi.org/10.1029/2018RG000596

Feldstein, S. B., & Franzke, C. (2006). Are the North Atlantic Oscillation and the northern annular mode distinguishable? *Journal of the Atmospheric Sciences*, *63*(11), 2915–2930. https://doi.org/10.1175/JAS3798.1

Fletcher, C. G., & Cassou, C. (2015). The dynamical influence of separate teleconnections from the Pacific and Indian Oceans on the northern annular mode. *Journal of Climate*, *28*(20), 7985–8002. https://doi.org/10.1175/JCLI-D-14-00839.1

Folland, C. K., Scaife, A. A., Lindesay, J., & Stephenson, D. B. (2012). How potentially predictable is northern European winter climate a season ahead? *International Journal of Climatology*, *32*(6), 801–818. https://doi.org/10.1002/joc.2314

Hall, R. J., Scaife, A. A., Hanna, E., Jones, J. M., & Erdélyi, R. (2017). Simple statistical probabilistic forecasts of the winter NAO. *Weather and Forecasting*, *32*(4), 1585–1601. https://doi.org/10.1175/WAF-D-16-0124.1

Hardiman, S. C., Dunstone, N. J., Scaife, A. A., Smith, D. M., Knight, J. R., Davies, P., et al. (2020). Predictability of European winter 2019/20: Indian ocean dipole impacts on the NAO. *Atmospheric Science Letters*, e1005. https://doi.org/10.1002/asl.1005

Hersbach, H., Bell, B., Berrisford, P., Hirahara, S., Horányi, A., Muñoz-Sabater, J., et al. (2020). The ERA5 global reanalysis. *Quarterly Journal of the Royal Meteorological Society*, *146*, 1999–2049. https://doi.org/10.1002/qj.3803

Hitchcock, P., & Simpson, I. R. (2014). The downward influence of stratospheric sudden warmings. *Journal of the Atmospheric Sciences*, *71*(10), 3856–3876. https://doi.org/10.1175/JAS-D-14-0012.1

Hurwitz, M. M., Newman, P. A., & Garfinkel, C. I. (2012). On the influence of North Pacific sea surface temperature on the Arctic winter climate. *Journal of Geophysical Research*, *117*, D19110. https://doi.org/10.1029/2012JD017819

Ineson, S., & Scaife, A. A. (2009). The role of the stratosphere in the European climate response to El Niño. *Nature Geoscience*, *2*(1), 32–36. https://doi.org/10.1038/ngeo381

Karpechko, A. Y., Charlton-Perez, A., Balmaseda, M., Tyrrell, N., & Vitart, F. (2018). Predicting sudden stratospheric warming 2018 and its climate impacts with a multimodel ensemble. *Geophysical Research Letters*, *45*, 13–538. https://doi.org/10.1029/2018GL081091

Lawrence, Z. D., Perlwitz, J., Butler, A. H., Manney, G. L., Newman, P. A., Lee, S. H., & Nash, E. R. (2020). The remarkably strong Arctic stratospheric polar vortex of winter 2020: Links to record-breaking Arctic Oscillation and ozone loss. *Journal of Geophysical Research: Atmospheres*, *125*, e2020JD033271. https://doi.org/10.1029/2020JD033271

Lee, S. H., Charlton-Perez, A. J., Furtado, J. C., & Woolnough, S. J. (2019). Abrupt stratospheric vortex weakening associated with North Atlantic anticyclonic wave breaking. *Journal of Geophysical Research: Atmospheres*, *124*, 8563–8575. https://doi.org/10.1029/2019JD030940

Manney, G. L., Livesey, N. J., Santee, M. L., Froidevaux, L., Lambert, A., Lawrence, Z., et al. (2020). Record-low Arctic stratospheric ozone in 2020: MLS observations of chemical processes and comparisons with previous extreme winters. *Geophysical Research Letters*, *47*, e2020GL089063. https://doi.org/10.1029/2020GL089063

NOAA (2020). National Centers for Environmental Information State of the Climate: Global Climate Report for February 2020. Retrieved 2020-06-30, from https://www.ncdc.noaa.gov/sotc/global/202002

Nie, Y., Scaife, A. A., Ren, H.-L., Comer, R. E., Andrews, M. B., Davis, P., & Martin, N. (2019). Stratospheric initial conditions provide seasonal predictability of the north atlantic and Arctic Oscillations. *Environmental Research Letters*, *14*, 34006. https://doi.org/10.1088/1748-9326/ab0385

Peings, Y. (2019). Ural blocking as a driver of early-winter stratospheric warmings. *Geophysical Research Letters*, *46*, 5460–5468. https://doi.org/10.1029/2019GL082097

Riddle, E. E., Butler, A. H., Furtado, J. C., Cohen, J. L., & Kumar, A. (2013). CFSv2 ensemble prediction of the wintertime Arctic Oscillation. *Climate Dynamics*, *41*(3–4), 1099–1116. https://doi.org/10.1007/s00382-013-1850-5

Rodwell, M. J., & Folland, C. K. (2002). Atlantic air-sea interaction and seasonal predictability. *Quarterly Journal of the Royal Meteorological Society*, *128*(583), 1413–1443. https://doi.org/10.1002/qj.200212858302

Scaife, A. A., Arribas, A., Blockley, E., Brookshaw, A., Clark, R. T., Dunstone, N., et al. (2014). Skillful long-range prediction of European and North American winters. *Geophysical Research Letters*, *41*, 2514–2519. https://doi.org/10.1002/2014GL059637

Scaife, A. A., Karpechko, A. Y., Baldwin, M. P., Brookshaw, A., Butler, A. H., Eade, R., et al. (2016). Seasonal winter forecasts and the stratosphere. *Atmospheric Science Letters*, *17*(1), 51–56. https://doi.org/10.1002/asl.598

Thompson, D. W. J., & Wallace, J. M. (1998). The Arctic Oscillation signature in the wintertime geopotential height and temperature fields. *Geophysical Research Letters*, *25*(9), 1297–1300. https://doi.org/10.1175/1520-0442(2004)017<3990:DCSOTN>2.0.CO;2

Thompson, D. W. J., & Wallace, J. M. (2001). Regional climate impacts of the Northern Hemisphere annular mode. *Science*, *293*(5527), 85–89. https://doi.org/10.1126/science.1058958

Trascasa-Castro, P., Maycock, A. C., Scott Yiu, Y. Y., & Fletcher, J. K. (2019). On the linearity of the stratospheric and Euro-Atlantic sector response to ENSO. *Journal of Climate*, *32*(19), 6607–6626. https://doi.org/10.1175/JCLI-D-18-0746.1

Wang, W., Anderson, B. T., Kaufmann, R. K., & Myneni, R. B. (2004). The relation between the North Atlantic Oscillation and SSTs in the north atlantic basin. *Journal of Climate*, *17*(24), 4752–4759. https://doi.org/10.1175/JCLI-3186.1

Wang, L., Ting, M., & Kushner, P. J. (2017). A robust empirical seasonal prediction of winter NAO and surface climate. *Scientific Reports*, *7*(1), 1–9. https://doi.org/10.1038/s41598-017-00353-y

Wilks, D. (2019). *Statistical Methods in the Atmospheric Sciences* (4th ed.). Amsterdam, Netherlands: Elsevier.

Wohltmann, I., von der Gathen, P., Lehmann, R., Maturilli, M., Deckelmann, H., Manney, G. L., et al. (2020). Near complete local reduction of Arctic stratospheric ozone by severe chemical loss in spring 2020. *Geophysical Research Letters*, *47*, e2020GL089547. https://doi.org/10.1029/2020GL089547